

Downlink Beamforming with Pinching-Antenna Assisted MIMO Systems

Ali Bereyhi Saba Asaad Chongjun Ouyang Zhiguo Ding H. Vincent Poor
University of Toronto York University Queen Mary University University of Manchester Princeton University
ali.bereyhi@utoronto.ca asaads@yorku.ca c.ouyang@qmul.ac.uk zhiguo.ding@manchester.ac.uk poor@princeton.edu

Abstract—Pinching antennas have been recently proposed as a promising flexible-antenna technology, which can be implemented by attaching low-cost pinching elements to dielectric waveguides. This work explores the potential of employing pinching antenna systems (PASs) for downlink transmission in a multiuser MIMO setting. We consider the problem of hybrid beamforming, where the digital precoder at the access point and the activated locations of the pinching elements are jointly optimized to maximize the achievable weighted sum-rate. Invoking fractional programming, a novel low-complexity algorithm is developed to iteratively update the precoding matrix and the locations of the pinching antennas. We validate the proposed scheme through extensive numerical experiments. Our investigations demonstrate that using PAS the system throughput can be significantly boosted as compared with the conventional fixed-location antenna systems, enlightening the potential of PAS as an enabling candidate for next-generation wireless networks.

I. INTRODUCTION

Shannon’s theory established the cornerstone of information theory and has significantly influenced the evolution of modern communication systems [1]. The conventional information-theoretic formulation of a communication system considers the channel between the transmitter and receiver to be determined by environmental factors, and hence to be beyond human control and manipulation. However, recent advances in communication technologies have challenged this assumption by introducing techniques with the capabilities to reconfigure channel parameters. An early example is the introduction of multiple-input multiple-output (MIMO) systems, which can modify the end-to-end channel by establishing parallel links between a pair of transmitter and receiver [2].

Recent developments in the area of flexible antenna design have provided more sophisticated means of channel reconfiguration. Technologies, such as reconfigurable intelligent surfaces (IRSs) [3], fluid antennas [4], and movable antennas [5], have provided significant degrees of freedom to control the effective end-to-end channel gain through their reconfigurable parameters. For example, IRSs reshape the wireless propagation environment in favor of signal transmission, such as bypassing obstructions, improving signal coverage, and reducing multi-user interference [6]. Another example is fluid antenna technology, which provides reconfigurability by employing a metallic or non-metallic liquid, e.g., Mercury or Galinstan, within a dielectric holder for signal transmission. This enables real-time adjustments to the shape and position of the antennas, making them suitable for compact devices with limited space [4]. The movable antenna technology enables

the localized movement of antenna elements in the transmitter/receiver array within designated regions, effectively using spatial degrees of freedom to improve wireless channel conditions in dynamic environments [5].

A. Pinching-Antenna Systems

Despite their promising theoretical gains in terms of system throughput, the integration aspect of the mentioned technologies remains challenging due to the need for real-time control, high cost and complexity, and limited ability to address large-scale path loss. Considering these challenges, several lines of research have focused on developing alternative reconfigurable technologies. The pinching antenna system (PAS) is one of the most recent proposals, which was originally proposed and demonstrated by NTT DOCOMO in 2022; see [7]–[9]. This innovative approach leverages low-cost dielectric materials, such as plastic clothespins, which can be applied at any point along a dielectric waveguide for radiation.

PASs offer flexibility in establishing or strengthening line-of-sight (LoS) links by activating pinching elements close to the serving user [8]. Unlike many earlier proposals, the tunable elements of PASs, i.e., pinching elements, can be implemented in a straightforward and low-cost manner. This has attracted several lines of recent research in the literature. The ergodic rate achieved by PAS was analyzed in the primary work [8] using stochastic geometry tools. The array gain achieved by PAS was examined in [10]. Several activation algorithms for optimizing the locations of pinching elements along a single waveguide were proposed in [11]–[13]. These studies collectively highlight the superiority of PAS over conventional fixed-location antenna systems in enhancing system throughput.

B. Contributions

The initial study in [8] has investigated the potential of PAS for MIMO communication, considering a simple two-user scenario. Motivated by their results, this work aims to study a gap that has not been explored in the earlier studies: the potential of PAS for general multiuser downlink transmission. To this end, we study the problem of multiuser beamforming through the following lines of contribution: (i) we formulate downlink transmission in a multiuser setting with multiple pinched waveguides as a classic vector Gaussian broadcast channel with a reconfigurable channel matrix. (ii) We propose a *hybrid* beamforming design in which the locations of the pinching elements and the digital precoding matrix are

designed jointly, such that the weighted achievable sum-rate is maximized. (iii) We develop a tractable iterative algorithm for the proposed joint design, which optimizes the digital precoding matrix at the transmitter and adjusts the locations of the pinching elements, simultaneously. Numerical simulations demonstrate that the proposed algorithm enables PAS-aided transmitter to achieve a significantly higher sum-rate, as compared with conventional fixed-location antenna systems, which highlights the great potential of this technology for improving the throughput of next-generation wireless systems.

Notation: Vectors, and matrices are shown by bold lower-case and bold upper-case letters, respectively. The transpose, conjugate and conjugate-transpose of \mathbf{H} are denoted by \mathbf{H}^T , \mathbf{H}^* and \mathbf{H}^H , respectively. The $N \times N$ identity matrix is shown by \mathbf{I}_N , and \mathbb{R} and \mathbb{C} denote the real axis and complex plane, respectively. For set $\{1, \dots, N\}$, we use shortened notation $[N]$. We denote expectation by $\mathbb{E}\{\cdot\}$, and $\mathcal{CN}(\eta, \sigma^2)$ is the complex Gaussian distribution with mean η and variance σ^2 . When the summation range is clear from the context, we omit it and denote only the index, e.g., \sum_k .

II. SYSTEM MODEL AND PROBLEM FORMULATION

Consider M dielectric waveguides, each equipped with a pinching element that can freely move across the waveguide. In practice, this can be realized via multiple elements, each covering one part of the waveguide. The element on each waveguide acts as an isotropic radiator whose signal is the phase-shifted version of the signal fed to the waveguide. Fig. 1 shows the configuration. We assume that waveguides are extended over the x -axis at the altitude a in an array formed on the y -axis with each two waveguides being distanced d . The location of the pinching element on the waveguide $m \in [M]$ is $\mathbf{v}_m = [\ell_m, (m-1)d, a]$, where ℓ_m is the position of the element on the waveguide m , assuming that the signal is fed to the waveguide at $[0, (m-1)d, a]$. Note that ℓ_m for $m \in [M]$ are the design parameters to be optimized.

The waveguides are fed by an access point (AP) that aims to serve K single-antenna users. The users are distributed within a known two-dimensional area, e.g., a square region. We denote the location of user $k \in [K]$ by $\mathbf{u}_k = [x_k, y_k, 0]$, assuming they are located in the xy -plane.

Let z_m denote the signal fed to waveguide m . The pinching element on this waveguide radiates a phase-shifted version of z_m . The radiated signal from the pinching elements can hence be represented as $t_m = \exp\{-j\theta_m\} z_m$, where θ_m denotes the phase-shift at the pinching element on the waveguide m and is determined by the location of the element. Noting that z_m is fed at location $\ell_m = 0$, at the carrier frequency f we can write $\theta_m = 2\pi i_{\text{ref}} |\ell_m| / \lambda$, where $\lambda = c/f$ denotes the wavelength with c being the speed of light, and i_{ref} is the reflective index of the waveguides. This indicates that the radiated signal is a function of ℓ_m , i.e., $z_m(\ell_m)$. We however drop this dependency for ease of notation.

A. Characterizing End-to-End Channel

Similar to [8], we assume that the users are in the LoS of the waveguides, which is typically the case in indoor

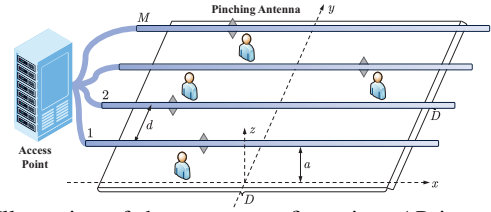


Fig. 1: Illustration of the system configuration: AP is equipped by multiple waveguides each pinched with an element.

settings. Furthermore, those non-LoS paths are assumed to be negligible since they are typically much weaker than those LoS paths. Let y_k denote the signal received by the user k . Considering LoS channels, we can write y_k as

$$y_k = \sum_m h_{m,k} t_m + \varepsilon_k, \quad (1)$$

where ε_k is complex zero-mean Gaussian noise with variance σ^2 , i.e., $\varepsilon_k \sim \mathcal{CN}(0, \sigma^2)$, and $h_{m,k} \in \mathbb{C}$ denotes the channel coefficient from the element on waveguide m to user k .

The channel coefficient $h_{m,k}$ can be explicitly expressed in terms of the location of the user and pinching element as [8]

$$h_{m,k} = \frac{\xi \alpha_{m,k}}{\|\mathbf{v}_m - \mathbf{u}_k\|} \exp\{-jk_0 \|\mathbf{v}_m - \mathbf{u}_k\|\}, \quad (2)$$

where $\xi = \lambda/4\pi$ is the coefficient proportional to the effective surface of the element, $k_0 = 2\pi/\lambda$ denotes the wavenumber, and $\alpha_{m,k}$ is the coefficient capturing shadowing between the pinching element on waveguide m and user k .

We note that the end-to-end channel between the waveguide array and the user k depends on the element locations. Defining $\mathbf{l} = [\ell_1, \dots, \ell_M]^T$, this means that the channel is a function of \mathbf{l} . Considering the radiation vector of waveguide m , we can write the channel to the user k as

$$y_k = \sum_m g_{m,k}(\mathbf{l}) z_m + \varepsilon_k = \mathbf{g}_k^T(\mathbf{l}) \mathbf{z} + \varepsilon_k, \quad (3)$$

where $\mathbf{z} = [z_1, \dots, z_M]$ denotes the transmitted beam by the array of waveguides, and $\mathbf{g}_k(\mathbf{l}) = [g_{1,k}(\ell_1), \dots, g_{M,k}(\ell_M)]^T$ with $g_{m,k}(\ell_m)$ being the effective channel between the waveguide m and the user k given by

$$\begin{aligned} g_{m,k}(\ell_m) &= h_{m,k} \exp\{-j\theta_m\} \\ &= \frac{\xi \alpha_{m,k} \exp\{-jk_0 (D_{m,k}(\ell_m) + i_{\text{ref}} \ell_m)\}}{D_{m,k}(\ell_m)}. \end{aligned} \quad (4b)$$

Here, $D_{m,k}(\ell_m)$ denotes the distance between the pinching element on the m -th waveguide and the user k , i.e.,

$$D_{m,k}^2(\ell_m) = (\ell_m - x_k)^2 + ((m-1)d - y_k)^2 + a^2. \quad (5)$$

Remark 1: The effective channel between the AP and user k can be decomposed as

$$\mathbf{g}_k(\mathbf{l}) = \mathbf{L}_k(\mathbf{l}) \mathbf{g}_k^0 \quad (6)$$

where $\mathbf{g}_k^0 = \xi[\alpha_{1,k}, \dots, \alpha_{M,k}]^T \in \mathbb{C}^M$ purely depends on the propagation environment and is independent of the element locations ℓ_1, \dots, ℓ_M . The matrix $\mathbf{L}_k(\mathbf{l})$ is further given by

$$\mathbf{L}_k(\mathbf{l}) = \text{diag} \left\{ \frac{\exp\{-jk_0 (D_{m,k}(\ell_m) + i_{\text{ref}} \ell_m)\}}{D_{m,k}(\ell_m)} \right\}_{m=1}^M \quad (7)$$

which depends on the location of pinching elements. Note that the channel in this case resembles the same model as in

IRS-assisted channels with a key difference: the channel of each user is modified by a phase-shift and attenuation that is *specific to the user*, i.e., $\mathbf{L}_k(\mathbf{l})$ depends on k . This difference comes from the fact that unlike reflecting surfaces, pinching elements can move a large range of distances.

B. Downlink Beamforming

Each waveguide is fed by a *single* signal, and the pinching elements can only modify the phase-shift by changing their location. When used in the form of an array, we can achieve multiplexing gain by performing transmit beamforming. Let $\mathbf{s} = [s_1, \dots, s_K]^T$ denote the collection of transmit signals the AP intends to send, with $s_k \in \mathbb{C}$ being the encoded information signal of user k . We assume that the signals are zero-mean unit-variance stationary processes satisfying $\mathbb{E}\{\mathbf{s}\mathbf{s}^H\} = \mathbf{I}$. The AP sets its feeding signal to each waveguide to be a linear combination of these signals, i.e., it sets $z_m = \tilde{\mathbf{w}}_m^T \mathbf{s}$ for some vector of coefficients $\tilde{\mathbf{w}}_m \in \mathbb{C}^K$ specified for waveguide m . The signal transmitted by the waveguide array can be represented as $\mathbf{z} = \mathbf{W}\mathbf{s}$ with $\mathbf{W} = [\tilde{\mathbf{w}}_1, \dots, \tilde{\mathbf{w}}_M]^T$ being the beamforming matrix. We further consider a power constraint on \mathbf{z} as $\mathbb{E}\{\|\mathbf{z}\|^2\} \leq P$ for some $P > 0$, which reduces to $\text{tr}\{\mathbf{W}\mathbf{W}^H\} \leq P$. The signal received by user k is given by

$$y_k = \mathbf{g}_k^T(\mathbf{l}) \mathbf{W}\mathbf{s} + \varepsilon_k, \quad (8)$$

which is a function of both \mathbf{W} and \mathbf{l} .

III. HYBRID BEAMFORMING DESIGN

In this setting, we can design the *digital* precoder \mathbf{W} and the *analog* parameter \mathbf{l} , jointly. This is a hybrid beamforming problem, which we discuss in the sequel.

To proceed with the beamforming design, let us first rewrite the received signal at user k as

$$y_k = \sum_j \mathbf{g}_k^T(\mathbf{l}) \mathbf{w}_j s_j + \varepsilon_k, \quad (9)$$

with \mathbf{w}_j denoting the j -th column vector of \mathbf{W} collecting the j -th entries of $\tilde{\mathbf{w}}_m$ for $m \in [M]$. We refer to \mathbf{w}_j as the *digital beamforming vector* of user j . The achievable rate of the user k in this case can be written as

$$R_k(\mathbf{W}, \mathbf{l}) = \log(1 + \text{SINR}_k(\mathbf{W}, \mathbf{l})), \quad (10)$$

where $\text{SINR}_k(\mathbf{W}, \mathbf{l})$ denotes the signal to interference and noise ratio (SINR) at user k given by

$$\text{SINR}_k(\mathbf{W}, \mathbf{l}) = \frac{|\mathbf{g}_k^T(\mathbf{l}) \mathbf{w}_k|^2}{\sum_{j \neq k} |\mathbf{g}_k^T(\mathbf{l}) \mathbf{w}_j|^2 + \sigma^2}. \quad (11)$$

The weighted sum-rate is then given by

$$\mathcal{R}(\mathbf{W}, \mathbf{l}) = \sum_k \lambda_k R_k(\mathbf{W}, \mathbf{l}), \quad (12)$$

for some weighting coefficient λ_k that are proportional to the expected quality of service for user k .

A. Optimal Beamforming Design

The ultimate goal of AP is to maximize the weighted sum-rate for a given power budget P and the physical limitations

of the waveguides. This can be formulated as

$$\max_{\mathbf{W}, \mathbf{l}} \mathcal{R}(\mathbf{W}, \mathbf{l}) \quad \text{s.t. } \text{tr}\{\mathbf{W}^H \mathbf{W}\} \leq P, \quad 0 \leq \ell_m \leq L_m, \quad (13)$$

where L_m denotes the length of the waveguide m .

The optimization in (13) is a non-convex problem whose global solution cannot be computed feasibly and is approximated with a local solution. We hence aim to develop an efficient suboptimal algorithm for this problem. To this end, we start with transforming the problem (13) into a *variational* form without the power constraint using the following lemmas.

Lemma 1: The optimal solution to the problem (13) satisfies the power constraint with equality, i.e., $\text{tr}\{\mathbf{W}_*^H \mathbf{W}_*\} = P$, for any \mathbf{W}_* that is a solution to (13).

Proof: The proof is concluded by contradiction: let $\hat{\mathbf{W}} = [\hat{\mathbf{w}}_1, \dots, \hat{\mathbf{w}}_K]$ be a solution to problem (13) that satisfies

$$\hat{P} \triangleq \text{tr}\{\hat{\mathbf{W}}^H \hat{\mathbf{W}}\} = \sum_j \|\hat{\mathbf{w}}_j\|^2 < P. \quad (14)$$

We now define the scaling factor $\rho = P/\hat{P}$ and the a scaled solution $\bar{\mathbf{w}}_j = \sqrt{\rho} \hat{\mathbf{w}}_j$. Note that the scaled beamforming matrix $\bar{\mathbf{W}} = [\bar{\mathbf{w}}_1, \dots, \bar{\mathbf{w}}_K]$ satisfies the power constraint with equality. Replacing into (11), it is readily shown that

$$\text{SINR}_k(\bar{\mathbf{W}}, \mathbf{l}) > \text{SINR}_k(\hat{\mathbf{W}}, \mathbf{l}), \quad (15)$$

for any \mathbf{l} . This means that $\bar{\mathbf{W}}$ achieves a larger sum-rate, which contradicts with the initial assumption. ■

Lemma 2: For a given \mathbf{l} , let $\bar{\mathbf{W}} = [\bar{\mathbf{w}}_1, \dots, \bar{\mathbf{w}}_K]$ denote a solution to the following problem

$$\max_{\mathbf{W}} \sum_k \lambda_k \log(1 + \overline{\text{SINR}}_k(\mathbf{W}, \mathbf{l})), \quad (16)$$

where $\overline{\text{SINR}}_k(\mathbf{W}, \mathbf{l})$ for $\mathbf{W} = [\mathbf{w}_1, \dots, \mathbf{w}_K]$ is defined as

$$\overline{\text{SINR}}_k(\mathbf{W}, \mathbf{l}) = \frac{|\mathbf{g}_k^T(\mathbf{l}) \mathbf{w}_k|^2}{\sum_{j \neq k} |\mathbf{g}_k^T(\mathbf{l}) \mathbf{w}_j|^2 + \frac{\sigma^2}{P} \sum_j \|\mathbf{w}_j\|^2}. \quad (17)$$

Then, a solution to (13) is determined from $\check{\mathbf{W}}$ as

$$\check{\mathbf{W}} = \sqrt{P/\text{tr}\{\bar{\mathbf{W}}^H \bar{\mathbf{W}}\}} \bar{\mathbf{W}}. \quad (18)$$

Proof: It is readily shown that the solution in (18) satisfies the power constraint with equality and that

$$\overline{\text{SINR}}_k(\check{\mathbf{W}}, \mathbf{l}) = \text{SINR}_k(\check{\mathbf{W}}, \mathbf{l}), \quad (19)$$

for any \mathbf{l} , which implies that the objective of (13) attains the same value as the one in (16). Noting that $\bar{\mathbf{W}}$ is a solution to (16), we can conclude that $\check{\mathbf{W}}$ maximizes the objective in (13) among all beamformers that satisfy the power constraint with equality. Lemma 1 further indicates that no solution with inequality constraint exists. This completes the proof. ■

Using Lemma 2, the optimal hybrid beamforming is equivalently determined by solving the following optimization

$$\max_{\mathbf{W}, \mathbf{l}} \bar{\mathcal{R}}(\mathbf{W}, \mathbf{l}) \quad \text{s.t. } 0 \leq \ell_m \leq L_m, \quad (20)$$

where $\bar{\mathcal{R}}(\mathbf{W}, \mathbf{l})$ is given by

$$\bar{\mathcal{R}}(\mathbf{W}, \mathbf{l}) = \sum_k \lambda_k \log(1 + \overline{\text{SINR}}_k(\mathbf{W}, \mathbf{l})) \quad (21)$$

with $\overline{\text{SINR}}_k(\mathbf{W}, \mathbf{l})$ being defined in (17).

B. Variational Solution via Fractional Programming

The variational problem in (20) describes maximizing sum of log ratios, whose solution can be efficiently approximated via fractional programming (FP) as outlined next [14], [15]. We start by defining \mathbb{S} to be the feasible set of the variational problem (20). Denoting $\mathbf{s} = (\mathbf{W}, \mathbf{l}) \in \mathbb{S}$, the Lagrange dual transform of (20) is given by

$$\mathcal{L}(\mathbf{s}, \boldsymbol{\omega}) = \sum_k \lambda_k (\log(1 + \omega_k) - \omega_k + \gamma(\mathbf{s}, \boldsymbol{\omega})), \quad (22)$$

where $\gamma(\mathbf{s}, \boldsymbol{\omega}) = (1 + \omega_k) |\mathbf{g}_k^T(\mathbf{l}) \mathbf{w}_k|^2 / \Gamma(\mathbf{s})$ with

$$\Gamma(\mathbf{s}) \triangleq \sum_j |\mathbf{g}_j^T(\mathbf{l}) \mathbf{w}_j|^2 + \frac{\sigma^2}{P} \sum_j \|\mathbf{w}_j\|^2. \quad (23)$$

The Lagrange duality implies that \mathbf{s}^* defined as

$$(\mathbf{s}^*, \boldsymbol{\omega}^*) = \operatorname{argmax}_{\mathbf{s} \in \mathbb{S}, \boldsymbol{\omega} \in \mathbb{R}_+^K} \mathcal{L}(\mathbf{s}, \boldsymbol{\omega}) \quad (24)$$

recovers the solution of (20), and that the optimal values of objectives in both problems are identical. Although the dual problem is not convex, its solution can be efficiently approximated via the block coordinate descent (BCD) algorithm [14], [15]. To this end, we initiate $\mathbf{s} = (\mathbf{W}, \mathbf{l})$ and iterate between the following two marginal problems:

- 1) For fixed $\mathbf{s} = (\mathbf{W}, \mathbf{l})$, we solve the marginal optimization

$$\boldsymbol{\omega}^* = \operatorname{argmax}_{\boldsymbol{\omega} \in \mathbb{R}_+^K} \mathcal{L}(\mathbf{s}, \boldsymbol{\omega}), \quad (25)$$

whose solution is given by

$$\omega_k^* = \overline{\operatorname{SINR}}_k(\mathbf{W}, \mathbf{l}). \quad (26)$$

- 2) We set $\omega_k = \omega_k^*$ and solve

$$\mathbf{s}^* = \operatorname{argmax}_{\mathbf{s} \in \mathbb{S}} \mathcal{L}(\mathbf{s}, \boldsymbol{\omega}^*), \quad (27)$$

which reduces to the problem of maximizing sum of fractions. This problem can be represented in quadratic form using the *quadratic transform* [14], [15].

To tackle the optimization in (27), we use the quadratic dual transform and rewrite the optimization as

$$\max_{\mathbf{s} \in \mathbb{S}, \mathbf{q} \in \mathbb{C}^K} \sum_k \lambda_k \left(2\sqrt{1 + \omega_k^*} \Re \{ q_k^* \mathbf{g}_k^T(\mathbf{l}) \mathbf{w}_k \} - |q_k|^2 \Gamma(\mathbf{s}) \right) \quad (28)$$

This dual problem has a quadratic objective with a smoother landscape and is optimized more efficiently. Note that the problem is still non-convex through the auxiliary variable \mathbf{q} , multiplicative expressions, and the functional form of $\mathbf{g}_k(\mathbf{l})$. We hence develop a two-tier BCD algorithm to approximate the solution of this quadratic problem.

C. Two-tier Iterative Algorithm

For brevity, we denote the multiuser downlink channel with $\mathbf{G}(\mathbf{l}) = [\mathbf{g}_1(\mathbf{l}), \dots, \mathbf{g}_K(\mathbf{l})]^T \in \mathbb{C}^{K \times M}$. We start with the outer loop, in which we use BCD to iteratively approximate \mathbf{q}^* . The outer tier iterates between these two steps:

- 1) Fix $\mathbf{s} = (\mathbf{W}, \mathbf{l})$ and solve (28) for \mathbf{q} . The solution to this problem is readily given by

$$q_k^* = \frac{\sqrt{1 + \omega_k^*} \mathbf{g}_k^T(\mathbf{l}) \mathbf{w}_k}{\Gamma(\mathbf{s})}. \quad (29)$$

- 2) Set $\mathbf{q} = \mathbf{q}^*$, and update \mathbf{s} by solving (28) for \mathbf{s} , i.e.,

$$\max_{\mathbf{W}, \mathbf{l}} F(\mathbf{W}, \mathbf{l}) \quad \text{with } 0 \leq \ell_m \leq L_m, \quad (30)$$

where the objective function, after a few lines of standard derivation, is represented as in (31) at the top of the next page. In (31), $\mathbf{T} = \mathbf{Q} \mathbf{A} \mathbf{A}$ and $\mathbf{U} = \mathbf{Q} \mathbf{A} \mathbf{Q}^H$ for diagonal matrices $\mathbf{A} = \operatorname{diag} \{ \lambda_k \}_{k=1}^K$, $\mathbf{Q} = \operatorname{diag} \{ q_k^* \}_{k=1}^K$, and $\mathbf{A} = \operatorname{diag} \{ \sqrt{1 + \omega_k^*} \}_{k=1}^K$.

The second marginal problem is non-convex, due to the multiplicative term $\mathbf{G}(\mathbf{l}) \mathbf{W}$. The problem is however marginally convex in both \mathbf{W} and $\mathbf{G}(\mathbf{l})$. We hence use the BCD algorithm once again to solve this marginal problem. The inner loop hence iterates between the following two steps:

- 1) Fix \mathbf{l} , and solve (30) for \mathbf{W} , which reduces to (32) given at the top of next page. This is standard regularized zero-forcing (RZF) precoding, whose solution is given by

$$\mathbf{W}^* = \left(\mathbf{G}^H(\mathbf{l}) \mathbf{U} \mathbf{G}(\mathbf{l}) + \frac{\sigma^2 \operatorname{tr} \{ \mathbf{U} \}}{P} \mathbf{I}_M \right)^{-1} \mathbf{G}^H(\mathbf{l}) \mathbf{T}, \quad (33)$$

and can be seen as RZF with an effective channel.

- 2) We next set $\mathbf{W} = \mathbf{W}^*$ and solve (30) marginally for \mathbf{l} .

In the second marginal optimization, the objective is given in terms of exponential sums, and hence its global optimum is not feasibly found. The classical approach to tackle these problems is to invoke greedy approaches. In the sequel, we develop a greedy approach based on the Gauss-Seidel scheme to efficiently approximate the solution of this marginal problem.

The Gauss-Seidel-based approach suggests to sequentially update the locations with each ℓ_m being updated individually treating the other locations as constants. In particular, by fixing $\ell_{m'}$ for $m' \neq m$, the scalar problem for ℓ_m is given by (34) at the top of next page, where $\tilde{\mathbf{G}}(\ell_m)$ is defined as

$$\tilde{\mathbf{G}}(\ell_m) = [\tilde{\mathbf{g}}_1, \dots, \tilde{\mathbf{g}}_{m-1}, \tilde{\mathbf{g}}_m(\ell_m), \tilde{\mathbf{g}}_{m+1}, \dots, \tilde{\mathbf{g}}_M], \quad (35)$$

with $\tilde{\mathbf{g}}_m(\ell_m) \in \mathbb{C}^{K \times 1}$ representing the m -th column of $\mathbf{G}(\mathbf{l})$ whose k -th entry is given by

$$[\tilde{\mathbf{g}}_m(\ell_m)]_k = \frac{\xi \alpha_{m,k} \exp \{ -jk_0 (D_{m,k}(\ell_m) + i_{\text{ref}} \ell_m) \}}{D_{m,k}(\ell_m)}. \quad (36)$$

Noting that $\ell_{m'}$ for $m' \neq m$ is treated as fixed, the argument $\ell_{m'}$ in $\tilde{\mathbf{g}}_{m'}$ for $m' \neq m$ is dropped for clarity. By simple lines of derivation, the problem in (34) can be rewritten as (37) on the top of next page, where \mathbf{a}_m is the m -th row of $\mathbf{W} \mathbf{T}^H$, and

$$\mathbf{b}_m^T = \sum_{m' \neq m} [\mathbf{W} \mathbf{W}^H]_{m,m'} \mathbf{h}_{m'}^H \mathbf{U}. \quad (38)$$

By denoting $\mathbf{c}_m = \mathbf{a}_m - \mathbf{b}_m$ and using the definition of $\tilde{\mathbf{g}}_m(\ell_m)$ given in (36), we can transform the objective function of the optimization (37) into (39) given at the top of next page, where $c_{m,k}$ is the k -th entry of \mathbf{c}_m , and $\angle z$ is the phase of z .

The optimization of ℓ_m is hence carried by classical scalar optimization, i.e., maximizing $f_m(\ell_m)$ in (39), within a fixed interval, which can be effectively solved via grid search.

Remark 2: It is worth mentioning that the classical gradient-based methods are not feasible for solving this scalar problem, since the objective function $f_m(\cdot)$ contains numerous stationary points caused by the oscillations of the cosine term.

$$F(\mathbf{W}, \mathbf{1}) = 2\Re \left\{ \text{tr} \left\{ \mathbf{T}^H \mathbf{G}(\mathbf{1}) \mathbf{W} \right\} \right\} - \text{tr} \left\{ \mathbf{G}(\mathbf{1}) \mathbf{W} \mathbf{W}^H \mathbf{G}^H(\mathbf{1}) \mathbf{U} \right\} - \frac{\sigma^2 \text{tr} \{ \mathbf{U} \}}{P} \text{tr} \{ \mathbf{W} \mathbf{W}^H \}, \quad (31)$$

$$\mathbf{W}^* = \underset{\mathbf{W} \in \mathbb{C}^{M \times K}}{\text{argmax}} \left\{ 2\Re \left\{ \text{tr} \left\{ \mathbf{T}^H \mathbf{G}(\mathbf{1}) \mathbf{W} \right\} \right\} - \text{tr} \left\{ \mathbf{W} \mathbf{W}^H \left(\mathbf{G}^H(\mathbf{1}) \mathbf{U} \mathbf{G}(\mathbf{1}) + \frac{\sigma^2 \text{tr} \{ \mathbf{U} \}}{P} \mathbf{I}_M \right) \right\} \right\}, \quad (32)$$

$$\max_{\ell_m} 2\Re \left\{ \text{tr} \left\{ \mathbf{T}^H \tilde{\mathbf{G}}(\ell_m) \mathbf{W} \right\} \right\} - \text{tr} \left\{ \mathbf{W} \mathbf{W}^H \tilde{\mathbf{G}}^H(\ell_m) \mathbf{U} \tilde{\mathbf{G}}(\ell_m) \right\} \text{ s.t. } 0 \leq \ell_m \leq L_m, \quad (34)$$

$$\max_{0 \leq \ell_m \leq L_m} 2\Re \left\{ \mathbf{a}_m^T \tilde{\mathbf{g}}_m(\ell_m) - \mathbf{b}_m^T \tilde{\mathbf{g}}_m(\ell_m) \right\} - [\mathbf{W} \mathbf{W}^H]_{m,m} \tilde{\mathbf{g}}_m^H(\ell_m) \mathbf{U} \tilde{\mathbf{g}}_m(\ell_m), \quad (37)$$

Algorithm 1 FP-BCD Algorithm

- 1: Choose a small ϵ and initialize \mathbf{W} and $\mathbf{1}$
 - 2: **repeat**
 - 3: Update ω_k and q_k using (26) and (29) for $k \in [K]$
 - 4: Update \mathbf{W} according to (33)
 - 5: Update ℓ_m by grid search for $m \in [M]$
 - 6: **until** increase of the objective in (13) falls below ϵ
 - 7: Scale \mathbf{W} as $\mathbf{W} = \sqrt{P/\text{tr} \{ \mathbf{W}^H \mathbf{W} \}} \mathbf{W}$
-

D. Overall Algorithm, Convergence, and Complexity

According to the solutions developed for each optimization block, the overall FP-BCD algorithm for solving problem (13) is given in Algorithm 1. Since the objective value is non-decreasing in each step of block coordinate descent and is bounded from above due to the power constraint, the convergence of Algorithm 1 is guaranteed. Furthermore, Algorithm 1 is computationally efficient, as the optimization variables in each step are updated by either the closed-form solution or the low-complexity one-dimensional search. It can be shown that the complexities of updating ω_k , q_k , \mathbf{W} , and ℓ_m in Algorithm 1 are in order of $\mathcal{O}(K^2M)$, $\mathcal{O}(K^2M)$, $\mathcal{O}(KM^2+M^3)$, and $\mathcal{O}(MLK)$, respectively. Hence, the overall complexity of Algorithm 1 scales with $\mathcal{O}(I(2K^2M+KM^2+M^3+MLK))$ with I being the number of iteration for the algorithm convergence.

IV. NUMERICAL INVESTIGATIONS

In this section, we validate the proposed algorithm through numerical experiments and compare it against the baseline.

Experimental Setting: The K users are assumed to be randomly and uniformly distributed within a square region with side length D , centered at $[D/2, D/2, 0]$, as illustrated in Fig. 1. Unless stated otherwise, the following parameters are used: the noise variance is set to $\sigma^2 = -90$ dBm, the waveguides are located at height $a = 3$ m and cover the entire area by being distanced as $d = \frac{D}{M-1}$ and of length $\ell_m \in [0, D]$, the carrier frequency is set to $f = 28$ GHz and the reflective index is set to $i_{\text{ref}} = 1.44$. We assume uniform weighting, i.e., $\lambda_k = 1/K$, and free-space path loss, i.e., $\alpha_{m,k} = 1$ for $m \in [M]$ and $k \in [K]$.

In the FP-BCD algorithm, the convergence threshold is set to $\epsilon = 10^{-3}$. For the one-dimensional grid search, we set the number of points to 10^3 . Since the performance of the FP-BCD algorithm may depend on the initial parameters, the digital beamformer is initialized using the maximal-ratio transmission (MRT) technique. The locations of the pinching elements are initialized based on a nearest-neighbor principle, where each ℓ_m is set to the location nearest to one of the users, i.e., $\ell_m = x_{k_m}$ for $m \in [M]$, where

$$k_m = \underset{k}{\text{argmin}} |y_k - (m-1)d|. \quad (40)$$

The numerical results are evaluated by averaging over 500 random channel realizations. For performance comparison, the conventional antenna system serves as the baseline, where M fixed-location antennas are deployed along the y -axis, centered within the square region. The antennas are half-wavelength spaced, with coordinates $[D/2, (m-1)\lambda/2, a]$ for $m \in [M]$.

Numerical Results: Fig. 2(a) shows the weighted sum-rate as a function of the maximum total transmit power, P , which compares the performance of PAS with the conventional fixed-location antenna system using the FP-BCD-based and zero-forcing (ZF)-based beamforming schemes. The results indicate that the sum-rate increases with P for all schemes. Notably, the PAS system can achieve significantly higher throughput than the conventional setting. To achieve the same sum-rate, the PAS requires considerably less transmit power. Specifically, a 6 dB performance gain is observed for the PAS in comparison with the baseline when FP-BCD algorithm is employed. This gain grows to 11 dB, when ZF beamforming is deployed at the conventional setting; see Fig. 2(a).

Fig. 2(b) depicts the sum-rate against the number of users K . The sum-rates achieved by both the proposed PAS setting and the baseline decrease monotonically as the number of users increases, primarily due to the rise in inter-user interference. Fig. 2(b) also highlights that the performance gain of PAS over the baseline grows with the increase in the side length D , i.e., as the area size increases. This demonstrates the unique capability of PAS to establish strong LoS links, as well as its capability to mitigate large-scale path-loss.

Fig. 2(c) further reinforces this observation by showing the sum-rate as a function of the side length of the square region.

$$f_m(\ell_m) = \sum_k \frac{\xi \alpha_{m,k} |c_{m,k}|}{D_{m,k}(\ell_m)} \left[2 \cos(k_0 (D_{m,k}(\ell_m) + i_{\text{ref}} \ell_m)) - \angle c_{m,k} - [\mathbf{W}\mathbf{W}^H]_{m,m} \xi \alpha_{m,k} \lambda_k |q_k|^2 / D_{m,k}(\ell_m) \right], \quad (39)$$

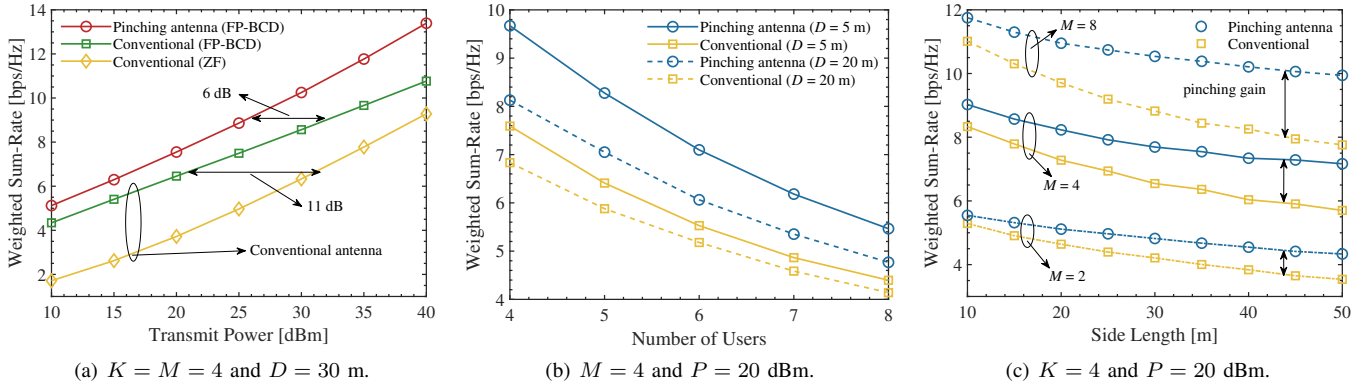


Fig. 2: Weighted sum-rate achieved by PAS. Arrows indicate the gain achieved by the proposed scheme over the fixed-antenna system.

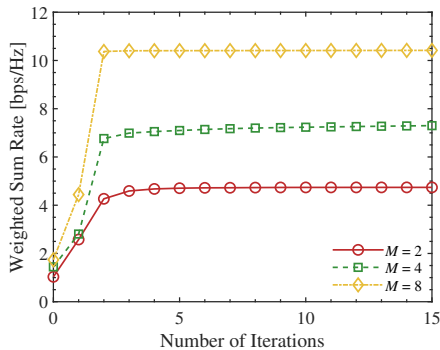


Fig. 3: Convergence of the proposed algorithm for different choices of M . Here, $P = 20$ dBm, $D = 30$ m, and $K = 4$.

As the side length increases, the performance gain of the PAS over the conventional baseline improves significantly. This is due to the fact that a larger side-length increases the average distance between users and the center, which results in higher path loss for the conventional setting. In contrast, the PAS can flexibly position its elements close to the users to reduce the distance and enhance the throughput.

Finally, Fig. 3 illustrates the convergence behavior of the proposed FP-BCD algorithm for different numbers of antenna elements, M . As observed, the weighted sum-rate gradually increases with more iterations and finally converges to a stable value for all considered values of M , which confirms the effectiveness of the proposed algorithm.

V. CONCLUSION

We studied downlink beamforming in a multiuser MIMO system, which deploys an array of pinched waveguides for transmission. A low-complexity joint beamforming design for this PAS-aided MIMO was developed, which invokes the principles of FP and BCD to alternatively optimize the digital beamformer at the AP and the activated locations of the pinching elements on the waveguides, aiming to maximize the achievable sum-rate. The effectiveness of the proposed design was validated through several numerical experiments.

The results of this study showcase the superiority of PAS-aided MIMO over conventional fixed-location designs, which together with its practicality highlight the potentials of PAS.

REFERENCES

- [1] C. E. Shannon, "A mathematical theory of communication," *Bell Syst. Tech. J.*, vol. 27, no. 3, pp. 379–423, Jul. 1948.
- [2] L. Lu, G. Li, L. Swindlehurst, A. Ashikhmin, and R. Zhang, "An overview of massive MIMO: Benefits and challenges," *IEEE J. Sel. Topics Signal Process.*, vol. 8, no. 5, pp. 742–758, 2014.
- [3] A. Beryhi, S. Asaad, C. Ouyang, R. R. Müller, R. F. Schaefer, and H. V. Poor, "Channel hardening of irts-aided multi-antenna systems: How should IRSs scale?" *IEEE J. Sel. Areas Commun.*, vol. 41, no. 8, pp. 2321–2335, 2023.
- [4] K.-K. Wong, A. Shojaefard, K.-F. Tong, and Y. Zhang, "Fluid antenna systems," *IEEE Trans. Wireless Commun.*, vol. 20, no. 3, pp. 1950–1962, Mar. 2021.
- [5] L. Zhu, W. Ma, and R. Zhang, "Movable antennas for wireless communication: Opportunities and challenges," *IEEE Commun. Mag.*, vol. 62, no. 6, pp. 114–120, Jun. 2024.
- [6] B. Zheng, C. You, and R. Zhang, "Double-IRS assisted multi-user MIMO: Cooperative passive beamforming design," *IEEE Trans. Wireless Commun.*, vol. 20, no. 7, pp. 13–26, Jul. 2021.
- [7] A. Fukuda, H. Yamamoto, H. Okazaki, Y. Suzuki, and K. Kawai, "Pinching antenna: Using a dielectric waveguide as an antenna," *NTT DOCOMO Tech. J.*, vol. 23, no. 3, pp. 5–12, 2022.
- [8] Z. Ding, R. Schober, and H. V. Poor, "Flexible-antenna systems: A pinching-antenna perspective," *arXiv preprint arXiv:2412.02376*, 2024.
- [9] Z. Yang, N. Wang, Y. Sun, Z. Ding, R. Schober, G. K. Karagiannidis, V. W. S. Wong, and O. A. Dobre, "Pinching antennas: Principles, applications and challenges," *arXiv preprint arXiv:2501.10753*, 2025.
- [10] C. Ouyang, Z. Wang, Y. Liu, and Z. Ding, "Array gain for pinching-antenna systems (PASS)," *arXiv preprint arXiv:2501.05657*, 2025.
- [11] Y. Xu, Z. Ding, and G. K. Karagiannidis, "Rate maximization for downlink pinching-antenna systems," *IEEE Wireless Commun. Lett.*, Submitted, 2024.
- [12] K. Wang, Z. Ding, and R. Schober, "Antenna activation for NOMA assisted pinching-antenna systems," *arXiv:2412.13969*, 2024.
- [13] S. A. Tegos, V. K. Papanikolaou, Z. Ding, and G. K. Karagiannidis, "Minimum data rate maximization for uplink pinching-antenna systems," *arXiv:2412.13892*, 2024.
- [14] K. Shen and W. Yu, "Fractional programming for communication systems—Part I: Power control and beamforming," *IEEE Trans. Signal Process.*, vol. 66, no. 10, pp. 2616–2630, May 2018.
- [15] —, "Fractional programming for communication systems—Part II: Uplink scheduling via matching," *IEEE Trans. Signal Process.*, vol. 66, no. 10, pp. 2631–2644, May 2018.